

Partial Conversion of *Hansenula polymorpha* Amine Oxidase into a “Plant” Amine Oxidase: Implications for Copper Chemistry and Mechanism[†]

Richard W. D. Welford,[‡] Angel Lam, Liviu M. Mirica, and Judith P. Klinman*

Departments of Chemistry and Molecular Cell Biology, University of California, Berkeley, California 94720-1460

Received May 17, 2007; Revised Manuscript Received July 10, 2007

ABSTRACT: The mechanism of the first electron transfer from reduced cofactor to O₂ in the catalytic cycle of copper amine oxidases (CAOs) remains controversial. Two possibilities have been proposed. In the first mechanism, the reduced aminoquinol form of the TPQ cofactor transfers an electron to the copper, giving radical semiquinone and Cu(I), the latter of which reduces O₂ (pathway 1). The second mechanism invokes direct transfer of the first electron from the reduced aminoquinol form of the TPQ cofactor to O₂ (pathway 2). The debate over these mechanisms has arisen, in part, due to variable experimental observations with copper amine oxidases from plant versus other eukaryotic sources. One important difference is the position of the aminoquinol/Cu(II) to semiquinone/Cu(I) equilibrium on anaerobic reduction with amine substrate, which varies from almost 0% to 40% semiquinone/Cu(I). In this study we have shown how protein structure controls this equilibrium by making a single-point mutation at a second-sphere ligand to the copper, D630N in *Hansenula polymorpha* amine oxidase, which greatly increases the concentration of the cofactor semiquinone/Cu(I) following anaerobic reduction by substrate. The catalytic properties of this mutant, including ¹⁸O kinetic isotope effects, point to a conservation of pathway 2, despite the elevated production of the cofactor semiquinone/Cu(I). Changes in $k_{\text{cat}}/K_{\text{m}}[\text{O}_2]$ are attributed to an impact of D630N on an increased affinity of O₂ for its hydrophobic pocket. The data in this study indicate that changes in cofactor semiquinone/Cu(I) levels are not sufficient to alter the mechanism of O₂ reduction and illuminate how subtle features are able to control the reduction potential of active site metals in proteins.

Copper amine oxidases (CAOs)¹ are ubiquitous enzymes catalyzing the conversion of primary amines to aldehydes, concomitant with the two-electron reduction of molecular oxygen to hydrogen peroxide (1, 2). The function of this reaction varies among species. For bacteria and yeast, CAOs enable the organism to use amines as a sole source of nitrogen (3), while for higher organisms these enzymes have been implicated in cellular functions that range from glucose homeostasis (4, 5) to adhesion of lymphocytes to endothelial cells (6).

The CAOs are homodimers of ca. ~70 kDa subunits and contain two cofactors per subunit, a Cu(II) center and 2,4,5-trihydroxyphenylalanine quinone (TPQ) (1). The TPQ cofactor is formed by an O₂-dependent post-translational modification of a tyrosine residue, catalyzed by the copper center, without the need for any additional proteins or cofactors (7). Since the identification of TPQ as the first

complex derivative of an amino acid side chain within the peptide backbone of a protein (8), CAOs have been the subject of extensive mechanistic and structural studies. Crystal structures are available for proteins from seven different sources, in a variety of complexes, with alternate metals and with site-specific mutations (9–12). Detailed kinetic studies both in the steady state and in the pre-steady state have also been completed (1, 2). In all cases, catalysis proceeds by a ping-pong mechanism. A general consensus has been reached on the mechanism for the first half-reaction, which involves conversion of amine to aldehyde (Scheme 1). A conserved catalytic base in the active site aids attack of the amine at the C-5 of the TPQ to form a substrate Schiff base; removal of the amine C- α proton by the same base is then driven by the gain of aromaticity in the cofactor. Hydrolysis of the resultant product Schiff base releases the aldehyde product to give the aminoquinol form of the cofactor (TPQ_{red}).

Contrastingly, two alternate mechanisms have been proposed for the reoxidation of TPQ_{red} by O₂ to regenerate TPQ_{ox} and yield H₂O₂ (13–15). The differences concern the nature of the first electron transfer to O₂. In pathway 1 (Scheme 1), an electron is transferred from TPQ_{red} to Cu(II), giving the semiquinone radical form of the cofactor (TPQ_{sq}) and Cu(I) (16, 17). Dioxygen is proposed to rapidly combine with Cu(I) to form copper(II) superoxide. Transfer of a second electron from TPQ_{sq}, and ultimately two protons, yields hydrogen peroxide and the oxidized iminoquinone form of the cofactor. Hydrolysis of the iminoquinone

[†] Supported by grants from the National Institutes of Health, GM 25765 to J.P.K. and GM078802 to L.M.M.

* To whom correspondence should be addressed; Phone: (510) 642-2668. Fax: (510) 643-6232. E-mail: klinman@berkeley.edu.

[‡] Present address: Biozentrum, University of Basel, Klingelbergstrasse 50/70, CH-4056 Basel, Switzerland.

¹ Abbreviations: CAO, copper amine oxidase; TPQ, 2,4,5-trihydroxyphenylalanine quinone; MeA, methylamine; TPQ_{red}, reduced aminoquinol form of TPQ; TPQ_{sq}, semiquinone form of TPQ; HPAO, *Hansenula polymorpha* CAO; $k_{\text{cat}}/K_{\text{m}}[\text{X}]$, the $k_{\text{cat}}/K_{\text{m}}$ value for substrate X; $^{\text{D}}(k_{\text{cat}}/K_{\text{m}})$, the ratio of $k_{\text{cat}}/K_{\text{m}}$ for protio and deuterio substrates; $^{\text{D}}(k_{\text{cat}}/K_{\text{m}})$, the ratio of $k_{\text{cat}}/K_{\text{m}}$ for protio and deuterio substrates; $^{18}(k_{\text{cat}}/K_{\text{m}})$, the ratio of $k_{\text{cat}}/K_{\text{m}}$ for ¹⁶O–¹⁶O and ¹⁶O–¹⁸O substrates; ¹⁸O KIE, oxygen-18 kinetic isotope effects.

respectively (32). Similarly, the second-order rate constants for reaction with O₂ at pH 7 tend to be at least an order of magnitude higher for the plant enzymes, with values of 10⁶ to 10⁷ M⁻¹ s⁻¹ reported (23, 32, 33). Finally, as mentioned previously the position of the TPQ_{red}/Cu(II) to TPQ_{sq}/Cu(I) equilibrium on anaerobic reduction with amine is highly variable, dependent on the enzyme source (16). At pH 7, the plant enzymes form around 40% TPQ_{sq}/Cu(I), while for the other eukaryotic enzymes the level is sufficiently small that it is difficult to detect and obtain an accurate measurement (23). Herein, we examine how the protein structure affects some of these differences, by using site-directed mutagenesis to partially convert HPAO into a plant-like CAO. We show that a simple increase in the level of TPQ_{sq}/Cu(I) is not sufficient to convert the pathway 2 mechanism to that of pathway 1. These results improve our understanding of the tuning of metal centers in proteins, in particular how a single side chain residue can affect both the redox properties and reactivity of metalloproteins.

MATERIALS AND METHODS

Mutagenesis. Mutations were made to the pDB20-HPAO plasmid (34). The ampicillin resistance gene enabled plasmid propagation to be carried out in *E. coli*. Site-directed mutagenesis was performed using the Stratagene Quick Change kit. Primers were purchased, HPLC-purified, from Operon. The forward primers are given below; the reverse primers were complementary to these. The mutated codon is given in bold and the changed bases are italic. The sequence of mutated plasmids was confirmed by automated DNA sequencing (University of California, Berkeley).

D630N:

5'-CCCAGCTCCTGAGA**ACTT**CCCATTTGATG-3'

Y407N:

5'-CTGCCAATTACGAGA**ACTGT**CTGTACTGGG-3'

Protein Expression and Purification. The pDB20-HPAO plasmid with WT-HPAO/mutant genes was transformed into the *Saccharomyces cerevisiae* cell line CG379 (ATCC) by lithium acetate chemical transformation. Proteins were purified by DEAE and size exclusion chromatography, giving proteins of >90% purity (by SDS-PAGE) according to published procedures (35).

ICP and EPR. ICP-AES was carried out on a Perkin-Elmer Optima 3000DV spectrometer analyzing the copper wavelengths 327.4, 324.8, and 224.7 nm and the zinc wavelengths 206.2, 213.9, and 202.5 nm.

EPR spectra were collected at 15 K using a Varian E9 spectrometer with a scan range of 1790–4790 G, microwave power of 5 mW, microwave of 9.2450 GHz, modulation amplitude of 20 G, and receiver gain of 32 000. A buffer blank spectrum was subtracted from the sample spectra before further processing.

UV-vis Spectroscopy. UV-vis spectra were collected on a Carey 50-Bio spectrometer, and the temperature was maintained using a Carey Peltier accessory. Generally, scans were recorded every 1 nm between 300 and 800 nm, a buffer blank was subtracted, and where appropriate the baseline was adjusted by taking an average of points between 770 and 800 nm.

Determination of the TPQ Content. The TPQ content was determined by titration with phenylhydrazine in 100 mM KP_i, pH 7.2, at 30 °C and measurement of the change in absorbance at λ = 448 nm using ε = 40 500 M⁻¹ cm⁻¹ (24). The concentration of TPQ per subunit was calculated using the total protein concentration, obtained from the Bio-Rad protein assay with bovine serum albumin standard and an MW of 75 700 for HPAO.

Copper Reconstitution of D630N. D630N was reconstituted with copper before kinetic and spectroscopic experiments as follows. Protein was diluted to 50 μM in 50 mM KP_i, pH 6.5, 1 equiv of CuSO₄ was then added, and the reaction was incubated overnight at room temperature. To remove any unbound copper, protein was repeatedly diluted and re-concentrated using Millipore 0.5 mL 50 000 MWCO spin concentrators, such that the effective dilution was >100-fold.

Steady-State Kinetics. Steady-state kinetic measurements were carried out by monitoring oxygen consumption using a Clark electrode and a YSI-5300 biological oxygen monitor. Standard conditions were as follows: a final volume of 1 mL, 25 °C, and initiation of reactions by addition of HPAO. For determinations of $k_{cat}/K_M[\text{MeA}]$ the oxygen concentration was kept constant at 258 μM, while for determinations of $k_{cat}/K_M[\text{O}_2]$ the methylamine (MeA) concentration was kept constant at 5 mM. Solutions were equilibrated to atmospheric conditions by stirring at 1000 rpm for 5 min just prior to initiation. For reactions at different oxygen concentrations, two flow meters were used to regulate the flow of O₂ and N₂, and the equilibration time was extended to 10 min. For assays in the pH ranges 6–8 and 8–9, 100 mM KP_i and 25 mM pyrophosphate buffers were used, respectively. The ionic strength of all buffers was kept constant at 0.3 M by addition of an appropriate amount of KCl. Data were fitted directly to the Michaelis–Menten equation, and k_{cat} was calculated using the active protein concentration as determined by phenylhydrazine titration. The value of $K_M[\text{O}_2]$ for D630N was difficult to measure and ranged from 0.5 to 1.5 μM. The lowest initial value of [O₂] we were able to obtain was 3.5 μM. Thus, to obtain $k_{cat}/K_M[\text{O}_2]$ with an error of less than 20%, many points were collected in the range of initial O₂ concentrations of 3.5–10 μM. At high pH the value of $k_{cat}/K_M[\text{O}_2]$ for D630N was especially difficult to measure, resulting in higher errors at pH values above 8. The maximum velocity and pK_a values were determined by fitting the data to one of eqs 1–4

$$\log(x) = \log(x_{\max}) - \log(1 + 10^{\text{p}K_{a1} - \text{pH}} + 10^{\text{p}K_{a1} + \text{p}K_{a2} - 2\text{pH}} + 10^{\text{pH} - \text{p}K_{a3}}) \quad (1)$$

$$\log(x) = \log(x_{\max}) - \log(1 + 10^{\text{p}K_{a1} - \text{pH}} + 10^{\text{pH} - \text{p}K_{a2}}) \quad (2)$$

$$\log(x) = \log(x_{\max}) - \log(1 + 10^{\text{p}K_{a1} - \text{pH}} + 10^{\text{p}K_{a1} + \text{p}K_{a2} - 2\text{pH}}) \quad (3)$$

$$\log(x) = \log(x_{\max}) - \log(1 + 10^{\text{p}K_a - \text{pH}}) \quad (4)$$

(24). In the equations, x represents either k_{cat} or $k_{cat}/K_M[\text{O}_2]$ and x_{\max} is the limiting value of x . Equation 1 fits a bell-shaped profile with two increasing pK_a values and one

decreasing pK_a value. Equation 2 fits a bell-shaped curve with one increasing pK_a value and one decreasing pK_a value. Equations 3 and 4 fit to two increasing pK_a values and one increasing pK_a value, respectively.

Anaerobic Reduction. Buffers for the different pH values were made as described in the Steady-State Kinetics section. Protein was exchanged into the appropriate buffer by a repeated dilution and concentration procedure using Millipore 0.5 mL 50 000 MWCO spin concentrators, such that the effective dilution was >100-fold. An 80 μ L volume of protein, at around 40 μ M in TPQ, was added to a cuvette with a ground glass joint and then sealed with a rubber septum. A Schlenk line apparatus with an argon cylinder attached to an Oxiclear disposable gas purifier was used to achieve anaerobiosis. Solutions were made anaerobic by passing a steady stream of Ar(g) into them while they were stirred for at least 30 min. During this period the vessel was briefly placed under vacuum a minimum of five times. Solutions containing proteins were not stirred, and Ar(g) was bubbled into the head space, rather than directly into the solution. Once anaerobiosis had been achieved, a UV-vis spectrum of the protein was taken. Then 2 μ L of an anaerobic solution of 40 mM MeA was added using a Hamilton gastight syringe. Spectra were then taken, with no further changes observed after the first spectrum in any case. This was followed by addition of 1 μ L of an anaerobic solution of 100 mM NaCN. In most cases all spectral changes occurred in the dead time (\sim 10 s) of the first spectrum. However, for experiments in which little TPQ_{sq} was observed on reduction with MeA, it took several minutes for the spectra to stop changing. A second addition of 1 μ L of 100 mM NaCN did not result in any further spectral changes in almost all cases. Again the exceptions were at low pH when no TPQ_{sq} was initially observed; in these cases up to seven 1 μ L additions of 100 mM NaCN were required to reach a point where the spectrum stopped changing.

To calculate the level of TPQ_{sq}/Cu(I), we used eq 5

$$\text{ratio} = [(A_{465} - A_{500})_{\text{reduced enzyme}} / (A_{465} - A_{500})_{\text{reduced enzyme} + \text{CN}}] - C \quad (5)$$

where A_y is the absorbance at wavelength y and C is a constant $[(A_{465} - A_{500})_{\text{reduced enzyme}} / (A_{465} - A_{500})_{\text{reduced enzyme} + \text{CN}}]$ calculated at the following pH values for different enzymes: WT-HPAO (pH 7), D630N (pH 6), Y407N (pH 8). The subtraction of C was necessitated by the different background absorbance differences observed between 465 and 500 nm for the different enzymes in the absence of TPQ_{sq}/Cu(I) formation.

¹⁸O Kinetic Isotope Effects. ¹⁸O KIEs were measured competitively as described previously (24, 36). Reactions with both WT-HPAO and D630N were carried out in 100 mM KP_i, pH 7.6, at 25 °C with 800 μ M O₂ and 3 mM MeA. The reaction was coupled with horseradish peroxidase (10 nM) using potassium ferrocyanide (3 mM) as the substrate to convert H₂O₂ to H₂O. The ¹⁸O/¹⁶O ratios were measured using isotopic ratio mass spectrometry (Krueger Enterprises, Cambridge, MA). The ¹⁸O KIEs are expressed as a ratio of ratios according to eq 6, where R_f is the ¹⁸O/¹⁶O isotopic ratio at f fractional conversion and R_0 is the isotopic ratio of the blank.

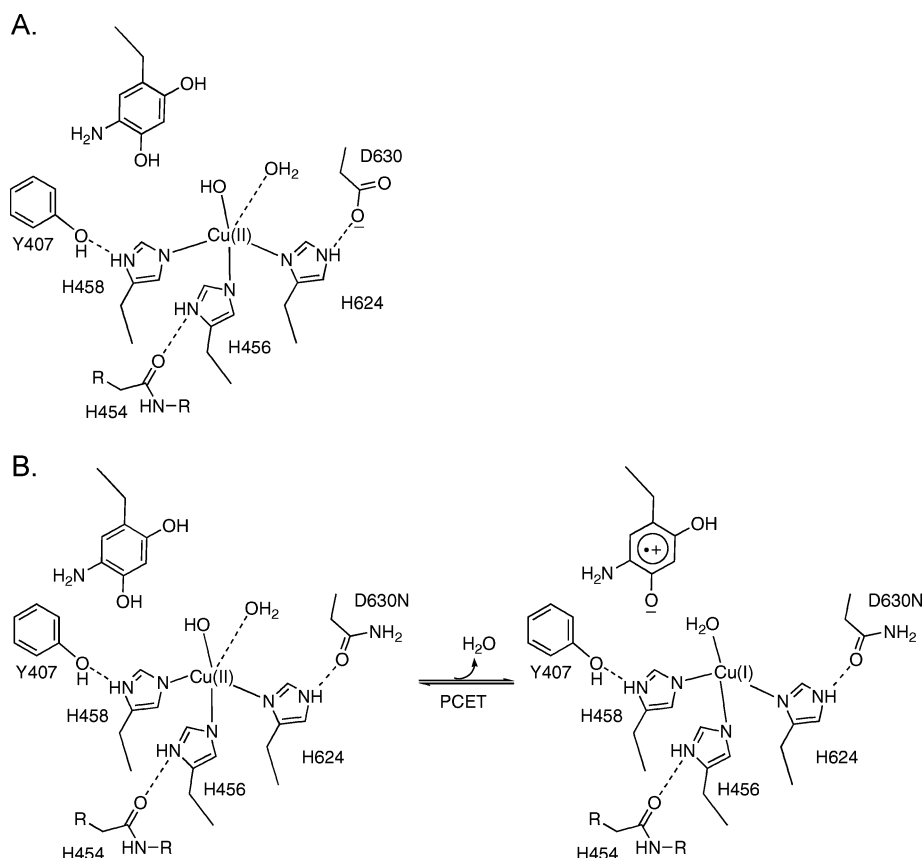
$$\frac{R_f}{R_0} = (1 - f)^{(1/^{18}\text{O KIE}) - 1} \quad (6)$$

Species That Accumulate in the Steady State. To examine which species accumulate in the steady state, a reaction was carried out in a cuvette with a ground glass joint at 25 °C. D630N was diluted to a final active enzyme concentration of 12 μ M in the cuvette with O₂-saturated buffer ([O₂] = 1170 μ M). The cuvette was then sealed with a rubber septum, and a steady stream of O₂ was passed into the headspace for 30 min. An initial spectrum, taking points every 2 nm, was recorded, after which MeA was added to a final concentration of 3 mM to initiate the reaction. Scans were then taken every 4.2 s.

RESULTS

Choice of Mutants. The initial aim of this study was to understand the structural factors that affect the position of the TPQ_{red}/Cu(II) to TPQ_{sq}/Cu(I) equilibrium. The potential for the 2-electron reduction of TPQ has been measured, with model compounds in solution (37) and for *A. globiformis* CAO (38). The reported values differ by only 60 mV, suggesting a comparative insensitivity of the cofactor potential to the environment. In comparison, the redox potential of copper in proteins is known to be sensitive to surrounding second-sphere amino acids. For example, up to 200 mV perturbation has been observed for the blue copper protein azurin (39, 40). Pertinently, EXAFS has shown that the primary copper coordination for both oxidized (5-coordinate) and dithionate-reduced (3-coordinate) enzyme forms is the same among CAOs from different sources (41). The sequences and structures of CAOs were compared to identify second-sphere residues to the copper that could alter the redox potential of the metal and, thus, the position of the equilibrium. In particular, we focused on differences between the plant and other eukaryotic CAOs. Y407 (using the numbering from HPAO, Scheme 2) was identified as a candidate residue, because it is conserved in 22 of 25 sequences, the exceptions being some plant CAOs where it is an asparagine (Supporting Information Figure 1). In the crystal structures of CAOs, Y407 (and equivalent residues) forms a hydrogen bond with the δ -N of the copper-coordinating His458 (Supporting Information Figure 2). We therefore focused on a Y407N mutation as the possible source of the differences between the plant enzymes and other CAOs. Additionally, another of the copper-ligating histidine residues, His624, forms a hydrogen bond with a conserved negatively charged residue, D630. D630 was mutated to asparagine to maintain the hydrogen-bonding capacity and size of the side chain, while removing the influence of a negative charge on the properties of the copper ion.

Protein Isolation and Initial Characterization. Mutant plasmids were made, and the protein was expressed and purified according to standard protocols (42). The Y407N mutant contained 0.7 TPQ/subunit and 0.9 Cu/subunit, similar to WT-HPAO (Table 1). In the initially purified D630N mutant, only about half of the copper sites were occupied and the percentage of active protein determined by phenylhydrazine titration was 10–12% instead of the usual 50%. The UV-vis spectra of D630N also contained

Scheme 2: Active Site Schematic Showing the Site of Conversion of WT-HPAO to D630N^a

^a Key: (A) based on the X-ray structure for HPAO (42), (B) replacement of D630N is proposed to alter the pK_a of the active site water and a subsequent proton-coupled electron transfer. Note that it is not definitively known whether Cu(I) is 3- or 4-coordinate (41).

Table 1: Cu and TPQ Contents per Subunit of HPAO As Determined by ICP-AES and Titration with Phenylhydrazine, Respectively

protein	Cu content	TPQ content
WT-HPAO	1.00 ± 0.05	0.56 ± 0.02
D630N	0.44 ± 0.01	0.12 ± 0.01
D630N + 1 equiv of Cu(II)	0.76 ± 0.03	0.23 ± 0.02
Y407N	0.86 ± 0.05	0.72 ± 0.09

absorption bands at 465 and 435 nm, similar to those observed for the TPQ_{sq} form of the cofactor (Figure 1A). The presence of TPQ_{sq} in the sample of D630N was confirmed by EPR spectroscopy, where a sharp feature at $g \approx 2$, ascribed to an organic radical, was observed (Figure 1B). Incubation of the purified protein with a stoichiometric amount of Cu(II) resulted in loss of the radical signal by both UV-vis and EPR (Figure 1B). Additionally, the level of bound copper was higher by ICP-AES, and the amount of active TPQ containing protein increased (Table 1). The broad UV-vis spectra of the Cu(II)-reconstituted D630N had a maximum at ~ 432 nm compared with the maximum at ~ 489 nm for WT-HPAO (cf. Figure 2); this may be due to changes in the charge distribution within the active site or to a mixture of TPQ conformations. Derivatization of the TPQ cofactor with phenylhydrazine to form the phenylhydrazone gave essentially identical final spectra for WT-HPAO, Y407N, and D630N (Figure 1C). The rate of formation of the phenylhydrazone was similar for WT-HPAO

($1.49 \pm 0.16 \text{ min}^{-1}$) and D630N ($1.16 \pm 0.23 \text{ min}^{-1}$), but was an order of magnitude lower for Y407N ($0.092 \pm 0.003 \text{ min}^{-1}$).

TPQ_{sq} is known to be stable in HPAO in aerobic conditions only in the absence of metal ($t_{1/2} = 564 \text{ min}^{-1}$, compared to $t_{1/2} = 2.6 \text{ min}^{-1}$ upon addition of Cu(II)) (25). For TPQ_{sq} to be present in the initially purified D630N mutant it seems likely that the subunits with TPQ_{sq} do not contain any Cu(II). The presence of TPQ_{sq} implies that D630N was probably catalytically active during expression/purification. Cu(II) is difficult to remove from CAOs (25), so it is likely that metal was lost as Cu(I) following electron transfer from TPQ_{red}. This implies that the Cu(I)/TPQ_{sq} would have a long enough lifetime for an in situ removal of Cu(I); in light of an expected rapid reaction of the Cu(I)/TPQ_{sq} with O₂, the available concentration of O₂ may have been quite low. The fact that addition of Cu(II) to purified D630N increases the TPQ/subunit ratio is, thus, attributed to oxidation of the reconstituted TPQ_{sq}/Cu(I) to yield the TPQ_{ox}/Cu(II) intermediate (cf. Supporting Information Scheme 1).

Effect of Mutations on the Reductive Half-Reaction. $k_{cat}/K_m[\text{MeA}]$, $D(k_{cat})$, and $D(k_{cat}/K_m[\text{MeA}])$. As catalysis by CAOs proceeds by a ping-pong mechanism, the value of k_{cat}/K_m for a methylamine substrate ($k_{cat}/K_m[\text{MeA}]$) is independent of the O₂ concentration and measures all steps involving MeA, up to the first chemically irreversible step. The values of $k_{cat}/K_m[\text{MeA}]$ were down by 3-fold and 40-fold for D630N and Y407N, respectively (Table 2). Inspection of the HPAO crystal structure (42) revealed that Y407 interacts with D319, the catalytic base for the reductive half-reaction through a

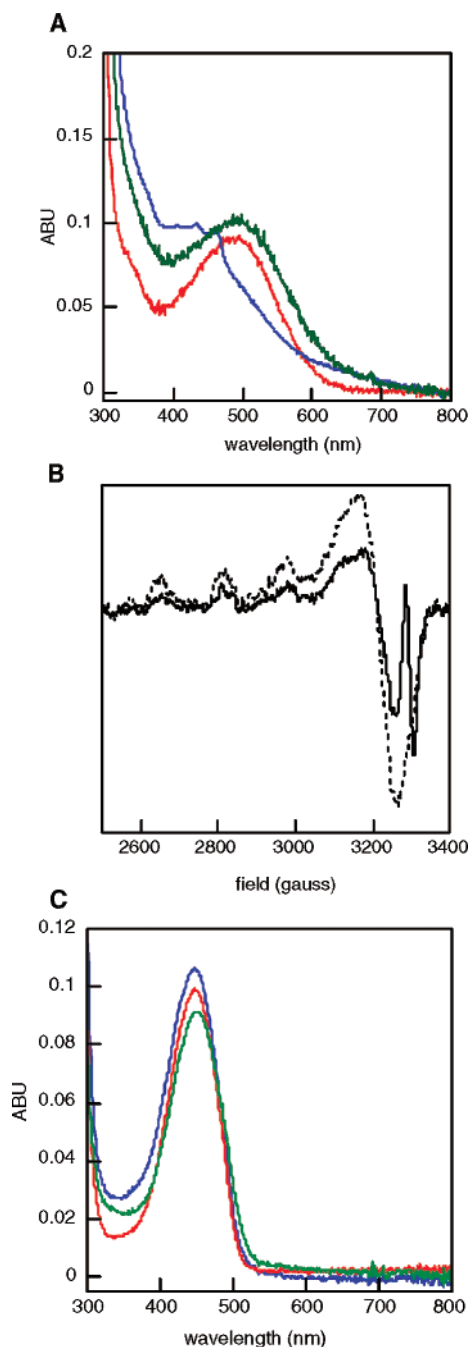


FIGURE 1: Spectroscopy of “as-purified” WT-HPAO, D630N, and Y407N. (A) UV-vis spectra of WT-HPAO (red), as-purified D630N (blue), and Y407N (green). (B) EPR spectra of D630N before (solid line) and after (dashed line) reconstitution with Cu(II). The g values for D630N were $g_{\perp} = 2.060$, $g_{\parallel} = 2.285$, and $A = 0.0172 \text{ cm}^{-1}$, and those for WT-HPAO were $g_{\perp} = 2.065$, $g_{\parallel} = 2.292$, and $A = 0.0167 \text{ cm}^{-1}$ (spectra not shown), the latter comparing favorably to published values. (C) UV spectra of phenylhydrazine-derivatized WT-HPAO (red), D630N (blue), and Y407N (green).

bridging water molecule. The loss of the bridging water may account for the difference in $k_{\text{cat}}/K_{\text{m}}[\text{MeA}]$ between Y407N and WT-HPAO, though this interaction is not present in all CAO structures and it is not known how the plant enzymes compensate for the loss of these hydrogen bonds. The small difference in $k_{\text{cat}}/K_{\text{m}}[\text{MeA}]$ for D630N is difficult to interpret, particularly in light of the distance of D630 from the site where the chemistry for the reductive half-reaction occurs.

The k_{cat} values for both the Y407N and D630N mutants were similar to that for WT-HPAO at pH 7.2, consistent with a step other than amine oxidation controlling k_{cat} and supported by the small $^{\text{D}}(k_{\text{cat}})$ values for WT-HPAO and D630N (Table 2). The isotope effect on the reductive half-reaction for D630N using CD_3NH_2 as the substrate is very similar to that of WT-HPAO, as expected from the small impact of D630N on $k_{\text{cat}}/K_{\text{m}}(\text{MeA})$.

Position of the $\text{TPQ}_{\text{red}}/\text{Cu(II)}$ to $\text{TPQ}_{\text{sq}}/\text{Cu(I)}$ Equilibrium. The effect of the mutations on the position of the $\text{TPQ}_{\text{red}}/\text{Cu(II)}$ to $\text{TPQ}_{\text{sq}}/\text{Cu(I)}$ equilibrium on anaerobic reduction with MeA was investigated. TPQ_{sq} has distinct features in the visible region of the spectrum at 360, 435, and 465 nm, along with an EPR signal due to its organic radical character (Figures 1A,B and 2A–C) (16). TPQ_{red} has an absorption feature at ca. 300 nm and does not absorb much above 350 nm. Additionally, the Cu(II) ion can be observed by EPR. Despite these spectroscopic signals, the absolute position of the equilibrium can be difficult to measure by EPR, as the TPQ_{sq} signal overlaps with that of Cu(II). A good estimate can be achieved by integration of the first hyperfine feature of the Cu(II) EPR spectra before and after reduction, with the change being correlated to $\text{TPQ}_{\text{sq}}/\text{Cu(I)}$ formation (17). Here we use a UV-vis method based on the observation that addition of cyanide to the anaerobic mixture of $\text{TPQ}_{\text{red}}/\text{Cu(II)}$ to $\text{TPQ}_{\text{sq}}/\text{Cu(I)}$ pulls the equilibrium to $\text{TPQ}_{\text{sq}}/\text{Cu(I)}$ (16). By comparing the 465 nm feature of TPQ_{sq} before and after addition of cyanide, we were able to directly observe the relative position of the equilibrium and to obtain a good estimate of its absolute value (Figure 2A–C). Using this method, we investigated the position of the equilibrium as a function of pH for both WT-HPAO and D630N (Figure 2D). In both cases the amount of $\text{TPQ}_{\text{sq}}/\text{Cu(I)}$ increased with pH, reaching a maximum of $\sim 15\%$ and $\sim 36\%$ for WT-HPAO and D630N, respectively. The difference was particularly stark at pH 7, where most investigators carry out their kinetic studies. For WT-HPAO the level of $\text{TPQ}_{\text{sq}}/\text{Cu(I)}$ was below the threshold of detection, while for D630N $\sim 22\%$ of the protein was found to be in the $\text{TPQ}_{\text{sq}}/\text{Cu(I)}$ form. In comparison, for Y407N $\text{TPQ}_{\text{sq}}/\text{Cu(I)}$ was undetectable at both pH 7.2 and pH 8 upon anaerobic reduction with methylamine. These differences show, first, how sensitive the redox potential of the active site copper ion is to the surrounding environment and, second, that we had achieved our first aim of altering the position of the $\text{TPQ}_{\text{red}}/\text{Cu(II)}$ to $\text{TPQ}_{\text{sq}}/\text{Cu(I)}$ equilibrium.

Impact of Mutations on Oxygen Reactivity. The apparent rate constant for reaction of the reduced form of D630N with O_2 , $k_{\text{cat}}/K_{\text{m}}[\text{O}_2]$, was measured as a function of pH and compared to the published data for WT-HPAO (Figure 3A) (24). The limiting value of $k_{\text{cat}}/K_{\text{m}}[\text{O}_2]$ was found to be ca. 4-fold higher for D630N than for WT-HPAO. The pK_a values of 6.8 and 7.9 for WT-HPAO have been assigned to the protonated aminoquinol and Cu(II)–OH₂, respectively (24). For the D630N mutant, the plateau was reached at a much lower pH and the data were fitted to only a single $\text{pK}_a = 7.2 \pm 0.1$. Notably, this implies a reduction of the higher pK_a , assigned to the Cu(II)–OH₂. At pH 7, where most biochemical studies are carried out, the value of $k_{\text{cat}}/K_{\text{m}}[\text{O}_2]$ was an order of magnitude higher for D630N than WT-HPAO. A faster $k_{\text{cat}}/K_{\text{m}}[\text{O}_2]$ is also observed for the plant enzymes at pH 7. For the Y407N mutant, $k_{\text{cat}}/K_{\text{m}}[\text{O}_2]$ was

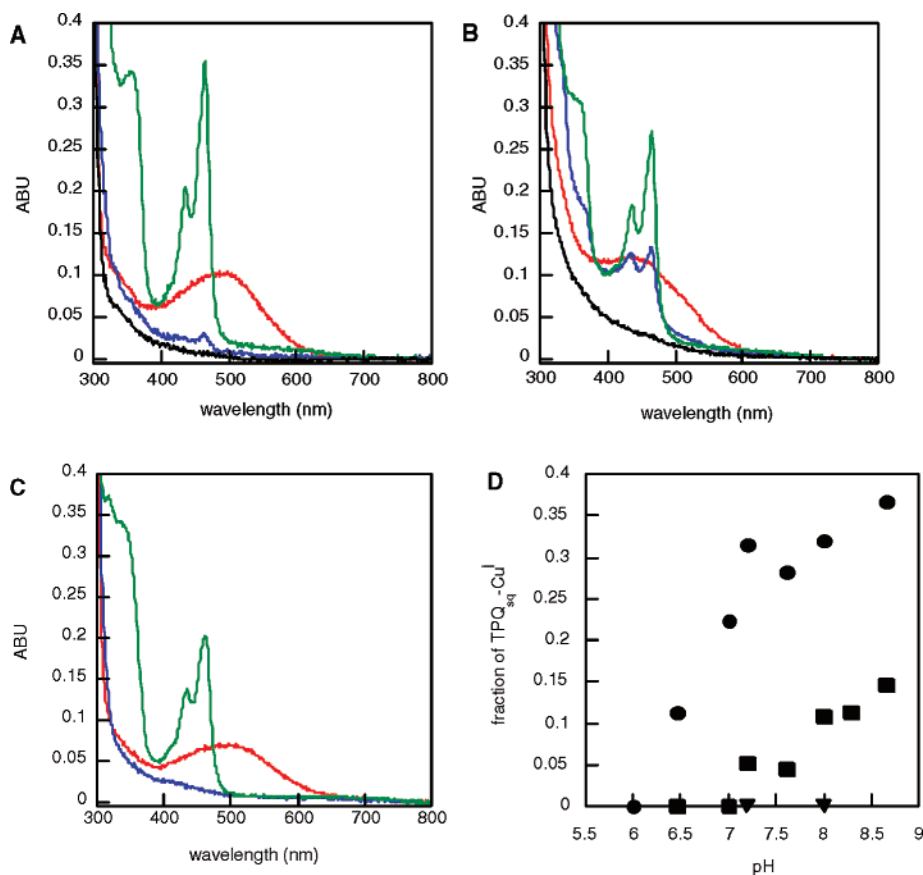


FIGURE 2: Anaerobic reduction of WT-HPAO, D630N, and Y407N with MeA substrate. (A), (B), and (C) are representative spectra of WT-HPAO (pH 7.2), D630N (pH 7.2), and Y407N (pH 8), respectively: oxidized protein (red), protein anaerobically reduced with MeA (blue), after addition of cyanide to the anaerobically reduced protein (green). Additionally, the spectra of anaerobically reduced WT-HPAO (pH 7) and D630N (pH 6) are shown in black, because at these pH values negligible $\text{TPQ}_{\text{sq}}/\text{Cu(I)}$ is formed. (D) pH dependence of $\text{TPQ}_{\text{red}}/\text{Cu(II)}$ to $\text{TPQ}_{\text{sq}}/\text{Cu(I)}$ equilibria for D630N (circles), WT-HPAO (squares), and Y407N (triangles).

Table 2: Kinetic Parameters for Reaction with a Methylamine Substrate, Determined at pH 7.2^a

protein	k_{cat} (s ⁻¹)	$k_{\text{cat}}/K_{\text{m}}[\text{MeA}]$ (10 ⁴ M ⁻¹ s ⁻¹)	^D (k_{cat})	^D ($k_{\text{cat}}/K_{\text{m}}[\text{MeA}]$)	¹⁸ ($k_{\text{cat}}/K_{\text{m}}[\text{O}_2]$)
WT-HPAO	1.7 ± 0.02	4.8 ± 0.9	1.3 ± 0.1	5.3 ± 1.1	1.011 ± 0.001 ^c
D630N	2.1 ± 0.04	1.5 ± 0.3	1.3 ± 0.1	5.9 ± 1.5	1.0074 ± 0.0004 ^c
Y407N	1.6 ± 0.23	0.25 ± 0.04	nd ^b	nd ^b	nd ^b

^a The values of ^D(k_{cat}), ^D($k_{\text{cat}}/K_{\text{m}}[\text{MeA}]$), and ¹⁸($k_{\text{cat}}/K_{\text{m}}[\text{O}_2]$) are the ratios of the values obtained with different isotopes as defined in the abbreviations footnote. ^b Not determined. ^c Determined at pH 7.6.

an order of magnitude lower than that for WT-HPAO at pH 7.2, 7.6, and 8 (Figure 3A).

The limiting rate, k_{cat} , of D630N was also measured as a function of pH and compared to the value obtained previously for WT-HPAO (Figure 3B). Though the limiting k_{cat} value for D630N was somewhat higher ((1.6 ± 0.5)-fold greater than for WT-HPAO), the differences are within experimental error. Mills et al. found two rate-increasing $\text{p}K_{\text{a}}$ values in k_{cat} for WT-HPAO of 6.1 and 7.7 and one rate-decreasing $\text{p}K_{\text{a}} = 8.7$ (24). Here, for D630N, we observed only a single increasing $\text{p}K_{\text{a}} = 7.72$ (±0.13) and a single decreasing $\text{p}K_{\text{a}} = 7.69$ (±0.14).

To address whether there were significant differences between D630N and WT-HPAO in the steps leading up to the first irreversible chemical step of the oxidative half-reaction, the ¹⁸O KIEs were measured. Competitive ¹⁸O KIEs were determined from the fractionation of oxygen isotopes, i.e., the change in ¹⁸O/¹⁶O during the consumption of O₂ catalyzed by either WT-HPAO or D630N. Isotope fractionation plots (¹⁸O/¹⁶O isotopic ratio of ratios versus fractional

conversion) for the reduction of O₂ by WT-HPAO and D630N using methylamine as the substrate are shown in Figure 4. The data are well fitted by eq 6 to give ¹⁸O KIE values of 1.011 ± 0.001 and 1.0074 ± 0.0004 for WT-HPAO and D630N, respectively. The former is close to the previously published value for WT-HPAO (24), though with greater precision. The results show clearly that changes in the oxygen bond order are occurring in the rate-determining step of $k_{\text{cat}}/K_{\text{m}}[\text{O}_2]$. The origin of the somewhat reduced KIE for D630N will be considered in detail in the Discussion.

Species That Accumulate in the Steady State. Taking advantage of the low $K_{\text{M}}[\text{O}_2]$ for D630N, we were able to monitor the UV-vis spectra in the steady state (Supporting Information Figure 3). Initiating the reaction with methylamine, there was an immediate (<10 s) bleaching of the absorbance at 500 nm, with no appearance of any features attributable to TPQ_{sq} within the limits of detection. On exhaustion of O₂ a sharp peak at 465 nm appeared assigned as TPQ_{sq} .

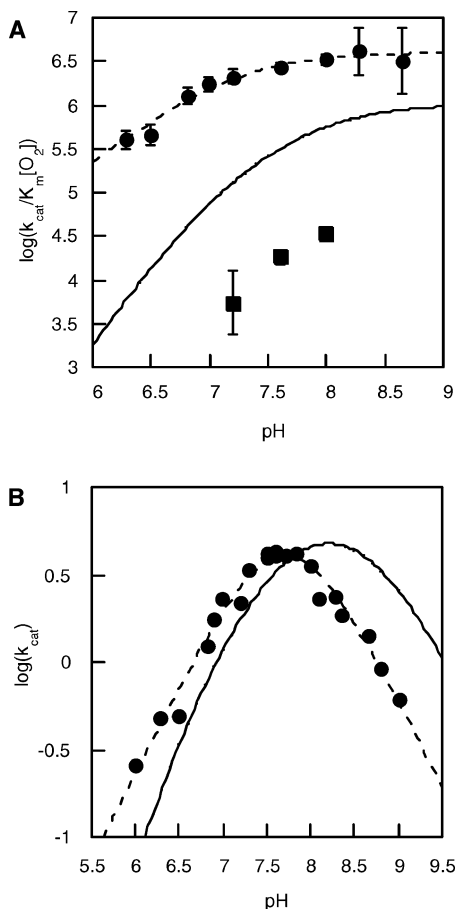


FIGURE 3: Variation of $k_{\text{cat}}/K_{\text{m}}[\text{O}_2]$ and k_{cat} with pH. (A) Variation of $k_{\text{cat}}/K_{\text{m}}[\text{O}_2]$ with pH: solid line, WT-HPAO; circles and dashed line, D630N; squares, Y407N. The solid line for WT-HPAO was plotted using eq 3, $\text{p}K_{\text{a}}$ values of 6.8 and 7.9, and a limiting $k_{\text{cat}}/K_{\text{m}}[\text{O}_2] = 1.04 \times 10^6 \text{ M}^{-1} \text{ s}^{-1}$ reported in a previous study (24). For D630N the data were fitted to eq 4, giving a single increasing $\text{p}K_{\text{a}} = 7.2 \pm 0.1$ with a limiting value of $k_{\text{cat}}/K_{\text{m}}[\text{O}_2] = (4.02 \pm 0.57) \times 10^6 \text{ M}^{-1} \text{ s}^{-1}$. Not enough points were measured for WT-HPAO to produce a full curve, but the values obtained were in good agreement with the earlier work. (B) Variation of k_{cat} with pH: solid line, WT-HPAO; circles and dashed line, D630N. For D630N the data were fitted to eq 2, giving a rate-increasing $\text{p}K_{\text{a}} = 7.72 \pm 0.13$, a decreasing $\text{p}K_{\text{a}} = 7.69 \pm 0.14$, and a limiting $k_{\text{cat}} = 12.6 \pm 3.6$. For WT-HPAO the line was plotted from eq 1 using the following values from a previous study, $\text{p}K_{\text{a}1} = 6.1$, $\text{p}K_{\text{a}2} = 7.7$, and $\text{p}K_{\text{a}3} = 8.7$, and a limiting $k_{\text{cat}} = 7.8 \pm 1.2$ (24).

Using the preferred amine substrate putrescine ($k_{\text{cat}} = 100 \text{ s}^{-1}$) and lentil seedling CAO, a steady-state mixture of TPQ_{ox} , $\text{TPQ}_{\text{sq}}/\text{Cu(I)}$, and $\text{TPQ}_{\text{red}}/\text{Cu(II)}$ has been reported (43). In the case of WT-HPAO, the absence of any detectable buildup of TPQ_{sq} in the steady state under conditions of saturating substrates, together with the partial rate limitation of k_{cat} for O_2 reduction, has argued against $\text{TPQ}_{\text{sq}}/\text{Cu(I)}$ being the catalytically reactive species (24). Although we do not know the extent to which O_2 reduction controls k_{cat} for D630N, the absence of detectable TPQ_{sq} provides support for a pathway 2 mechanism for D630N analogous to WT-HPAO.

DISCUSSION

Impact of Mutations on Measured Parameters and Their pH Dependencies. By making a single-point mutant in the second sphere of the copper ion of HPAO, we were able to

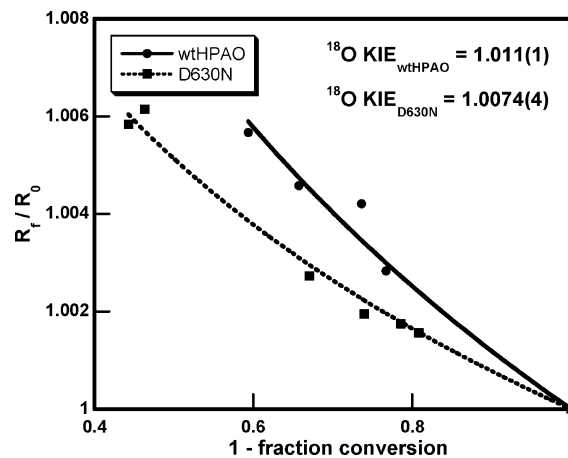


FIGURE 4: Isotope fractionation plots for WT-HPAO (circles) and D630N (squares) (25 °C, pH 7.6). ^{18}O KIE values were obtained by fitting to eq 6.

convert the enzyme into a “plant-like” CAO. Similar to plant CAOs, D630N-HPAO forms large quantities of $\text{TPQ}_{\text{sq}}/\text{Cu(I)}$ on anaerobic reduction with amine and reacts with O_2 an order of magnitude faster than WT-HPAO at pH 7. However, the limiting rate constant, k_{cat} , of D630N ($12.6 \pm 3.6 \text{ s}^{-1}$) is similar to that of WT-HPAO ($7.8 \pm 1.2 \text{ s}^{-1}$), not the elevated value observed with plant CAOs ($\sim 150 \text{ s}^{-1}$). The Y407N mutant had the opposite effect of D630N. The rate of reaction with O_2 is down an order of magnitude compared to that of WT-HPAO, and no $\text{TPQ}_{\text{sq}}/\text{Cu(I)}$ was observed on anaerobic reduction, even at pH 8. Collectively these data help to explain the disparate experimental observations with different CAOs and show how the active site copper reactivity is highly dependent on the second-sphere residues.

The k_{cat} and $^{\text{D}}(k_{\text{cat}})$ values are nearly identical for both D630N and WT-HPAO, indicating that the reductive half-reaction and the nature of the rate-limiting step(s) are unlikely to have changed greatly. Previously, stopped-flow experiments were used to determine the steps that contribute to k_{cat} for WT-HPAO (44). Three steps were found to contribute dominantly to rate limitation and were assigned as follows: aldehyde release (27.9 s^{-1}), reduction of O_2 (22.1 s^{-1}), and peroxide release (13.1 s^{-1}). If the observed 4-fold limiting increase in $k_{\text{cat}}/K_{\text{m}}[\text{O}_2]$ for D630N is applied to reduction of O_2 by the reduced enzyme, an increase in the limiting value of k_{cat} from 6.4 to 7.9 s^{-1} would be expected.² This is an increase of 1.4-fold and is similar in magnitude to our observed value of 1.6 ± 0.5 ($12.6 \text{ s}^{-1}/7.8 \text{ s}^{-1}$), though the values are within experimental error of one another. Comparing Co(II)-substituted HPAO with WT-HPAO, the limiting values of k_{cat} are again similar (2.1 and 7.8 s^{-1} , respectively), but the $k_{\text{cat}}/K_{\text{m}}[\text{O}_2]$ is 245-fold lower for the cobalt-substituted enzyme (25). If we assume, in a similar manner, that the oxidation of reduced enzyme is 245-fold lower, we predict the rate-limiting value of k_{cat} to be 72-fold higher for WT-HPAO in relation to the cobalt-substituted enzyme. This is in sharp contrast to the experimentally determined values, which differ by only a factor of 3.7. The k_{cat} of Co(II)-substituted lentil seedling CAO is reported to be 11 s^{-1} (29), again indicating that catalysis can proceed at a considerable

² Calculated according to $1/k_{\text{cat}} = 1/k_1 + 1/k_2 + 1/k_3$, where the rate constants refer to aldehyde release, oxygen reduction, and peroxide release, respectively.

rate in the absence of TPQ_{sq}/Cu(I). What is clear from comparing WT-HPAO, Co(II)-HPAO and D630N-HPAO is that the changes in k_{cat} are relatively small compared to the collective differences in $k_{\text{cat}}/K_{\text{m}}[\text{O}_2]$ and the amount of TPQ_{sq}/Cu(I) formed upon anaerobic reduction by substrate. This argues that the mechanism of reduction of bound O₂ is similar among these three forms of HPAO.

We note that stopped-flow experiments on lentil seedling CAO have defined the rate-limiting step as hydrolysis of the product Schiff base to release the aldehyde product (15). Clearly, the superior k_{cat} of the plant CAO implicates not just an increased rate for the oxidative half-reaction, but also a faster product release step. The impact of modest changes in the active site of the CAOs can be manifested on numerous steps, making it essential to measure as many parameters as possible, as done here and in earlier studies of HPAO.

The pH dependence of TPQ_{sq}/Cu(I) formation on anaerobic reduction with amine substrates has been measured for several different CAOs. For HPAO, D630N-HPAO, bovine serum CAO, and *A. globiformis* CAOs a trend of increasing levels of TPQ_{sq}/Cu(I) with pH is observed in the range of 6–8 (17, 23). In comparison, lentil seedling and *E. coli* CAOs show a bell-shaped profile (33, 45). For lentil seedling CAO, WT-HPAO, and D630N-HPAO the pH dependence of TPQ_{sq}/Cu(I) has been shown to follow the same profile as the second-order rate constant for reaction of O₂ (33). One mechanistic aspect that became particularly clear during this study was that the enzyme form that reacts by pathway 2 (containing neutral TPQ_{red} and Cu(II)-OH, Scheme 2) will also be the form of the enzyme that favors formation of TPQ_{sq}/Cu(I). The conversion to TPQ_{sq}/Cu(I) is expected to proceed by proton-coupled electron transfer from TPQ_{red} to Cu(II)-OH, giving TPQ_{sq} and Cu(I)-OH₂. Similarly, for pathway 2 (Scheme 1) direct electron transfer from TPQ_{red} to O₂ is expected to be accompanied by a subsequent rapid proton transfer to Cu(II)-OH to generate Cu(II)-OH₂ (23). The water, thus formed, is shown as undergoing displacement by O₂^{•-}, to produce the inner-sphere complex, Cu(II)-O₂^{•-}. Importantly, we conclude that comparative pH dependencies for $k_{\text{cat}}/K_{\text{m}}[\text{O}_2]$ versus TPQ_{sq}/Cu(I) formation cannot, in themselves, be used to discriminate between the postulated O₂ reduction mechanisms in Scheme 2.

The demonstration herein that the D630N mutation alters the pH dependencies for both $k_{\text{cat}}/K_{\text{m}}[\text{O}_2]$ and the position of the TPQ_{red}/Cu(II) to TPQ_{sq}/Cu(I) equilibrium is attributed to a reduction in the pK_a of the Cu(II)-OH₂. These observations can be rationalized in terms of the effect of the mutation on the electron-donating ability of His624 (Scheme 2). An asparagine at position 630 will lead to a decreased electron-donating ability of His624, making it easier to deprotonate Cu(II)-OH₂ in the mutant relative to the WT. The same feature that affects the pK_a at the Cu(II)-OH₂ may also be expected to increase the redox potential of the metal, offering an explanation for the substantial increase in the level of the TPQ_{sq}/Cu(I).

Mechanism of O₂ Reduction and Origin of the Increase in $k_{\text{cat}}/K_{\text{m}}[\text{O}_2]$ for D630N-HPAO. In the context of Scheme 1, two alternate explanations were possible for the observed 4-fold increase in $k_{\text{cat}}/K_{\text{m}}[\text{O}_2]$ for D630N-HPAO over WT-HPAO: either a change in reaction mechanism or a change in O₂ affinity at the active site. Competitive ¹⁸O kinetic isotope effects, ¹⁸($k_{\text{cat}}/K_{\text{m}}[\text{O}_2]$), were carried out in an effort

to distinguish these possibilities, revealing the extent to which a change in oxygen bond order occurs in all reversible steps up through the first irreversible step. Previously, the ¹⁸O KIEs have been measured for WT-HPAO, HPAO-Co(II), and bovine serum CAO at pH 6.0, 7.2, and 8.5, with all values being essentially the same (1.010 ± 0.002), identifying electron transfer to O₂ as a rate-limiting step (23, 24). The reduction in the size of the observed ¹⁸O KIEs in relation to a calculated (24, 36) value of 1.03 for an outer-sphere conversion of O₂ to O₂^{•-} could have been the result of oxygen binding being partially rate-determining; however, studies of the impact of solvent viscosity on $k_{\text{cat}}/K_{\text{m}}[\text{O}_2]$ were concluded to rule out this interpretation. Alternative possibilities that have been considered are the presence of an internal commitment that controls the binding of O₂^{•-} to the Cu(II) center or an interaction between the active site Cu(II) ion with O₂^{•-} as it is formed during the reduction of O₂ by the TPQ cofactor (1). We favor the former process in which O₂^{•-} binding to Cu(II) is partially rate-determining, thus lowering the observed ¹⁸O KIE. The change in the properties of D630N (a lowered reduction potential together with an altered pK_a for one of the metal-bound waters) may be expected to alter the degree to which a second step is partially rate-determining. Roth has, in fact, suggested that either superoxide collapse onto the Cu(II) center or the second electron transfer to a Cu(II)(O₂^{•-}) intermediate from the TPQ_{sq} could be rate-determining for $k_{\text{cat}}/K_{\text{m}}[\text{O}_2]$ in HPAO (46). Turning to pathway 1 of Scheme 1, available ¹⁸O KIEs for direct reaction of O₂ with Cu(I) indicate changes in bond order that are significantly larger than suggested by an ¹⁸O KIE value of 1.01, with measured and calculated equilibrium values for Cu(I) + O₂ ⇌ Cu(II)-O₂^{•-} of 1.015–1.023 (46). The fact that the observed ¹⁸O KIE for D630N is *smaller* than for WT-HPAO argues strongly against a change in mechanism from pathway 2 to pathway 1, despite the large increase in TPQ_{sq}/Cu(I) seen in the reduced form of the D630N mutant. In the case of the D630N mutant, a reduced electron-donating ability that both increases the redox potential of the copper center and stabilizes a Cu(II)-OH center relative to Cu(II)-OH₂ may also lead to a stronger interaction between the Cu(II) center and O₂^{•-} in the course of its formation; the latter could well be the origin of the somewhat decreased experimental ¹⁸O KIE. As discussed below, the reduction in charge that occurs within the active site of D630N may also be expected to increase the affinity of O₂ for its site; this could produce a somewhat larger barrier for the loss of O₂ from its binding pocket, making substrate dissociation partially rate-limiting and the experimental ¹⁸O KIE smaller than for WT-HPAO.

The evidence for the plausibility of pathway 2 from studies of Co(II)-substituted CAOs remains strong (24, 26–29). Combining the data here and our earlier work on HPAO (24), we have collected some of the most detailed studies concerning trends in the TPQ_{red}/Cu(II) to TPQ_{sq}/Cu(I) equilibrium and $k_{\text{cat}}/K_{\text{m}}[\text{O}_2]$ with pH. On face value the similar trends with pH might have offered the conclusion that TPQ_{sq}/Cu(I) is the active species. However, the data offer no definitive proof that TPQ_{sq}/Cu(I) is catalytically competent, as its formation will be favored by the same factors that favor reaction of TPQ_{red}/Cu(II) with O₂. Overall, the metal substitution data, together with measured ¹⁸O kinetic isotope effects, implicate a conservation of pathway 2 of

Scheme 2, independent of the change in the redox potential of the active site copper ion.

In light of the above discussion, we now examine in greater detail the 4-fold elevation for $k_{\text{cat}}/K_{\text{m}}[\text{O}_2]$ in the D630N mutant. The fact that the increase in $\text{TPQ}_{\text{sq}}/\text{Cu(I)}$ and increase in $k_{\text{cat}}/K_{\text{m}}[\text{O}_2]$ are close in magnitude must be considered in the context that $\text{TPQ}_{\text{red}}/\text{Cu(II)}$ and $\text{TPQ}_{\text{sq}}/\text{Cu(I)}$ are expected to be in rapid equilibration. Using eqs 7–9, it can be shown that a ca. 2.6-fold increase in $\text{TPQ}_{\text{sq}}/\text{Cu(I)}$ (at the highest pH, Figure 2D) would only increase $k_{\text{cat}}/K_{\text{m}}[\text{O}_2]$ by ca. 2.2-fold in the event that $\text{TPQ}_{\text{sq}}/\text{Cu(I)}$ were the active species.

$$K_{\text{eq}} = \frac{[\text{ETPQ}_{\text{sq}}/\text{Cu(I)}]}{[\text{ETPQ}_{\text{red}}/\text{Cu(II)}]}$$

$$k_{\text{cat}}/K_{\text{m}}[\text{O}_2] \propto [\text{ETPQ}_{\text{sq}}/\text{Cu(I)}] \quad (7)$$

$$E_{\text{T}} = [\text{ETPQ}_{\text{red}}/\text{Cu(II)}] + \frac{[\text{ETPQ}_{\text{sq}}/\text{Cu(I)}]}{[\text{ETPQ}_{\text{sq}}/\text{Cu(I)}](K_{\text{eq}} + 1)/K_{\text{eq}}} \quad (8)$$

$$\frac{(k_{\text{cat}}/K_{\text{m}}[\text{O}_2])_{\text{D630N}}}{(k_{\text{cat}}/K_{\text{m}}[\text{O}_2])_{\text{WT}}} = \frac{((K_{\text{eq}} + 1)/K_{\text{eq}})_{\text{WT}}}{((K_{\text{eq}} + 1)/K_{\text{eq}})_{\text{D630N}}} = 2.2 \quad (9)$$

The most reasonable interpretation of the observed 4-fold increase in $k_{\text{cat}}/K_{\text{m}}[\text{O}_2]$ for D630N is that the resulting reduction in active site charge in D630N enhances the prebinding of O_2 within its hydrophobic pocket adjacent to the copper site. A similar argument has been invoked to explain the reduction in $k_{\text{cat}}/K_{\text{m}}[\text{O}_2]$ for the Co(II)-substituted form of HPAO without any change in k_{cat} , ascribed in that case to a significant elevation of the net charge at the active site that accompanies the perturbed $\text{p}K_{\text{a}}$ for Co(II)–OH₂.

CONCLUSION

The results reported herein show how a second-sphere single-point mutation affects the properties of a redox-active metalloenzyme. First, we have demonstrated that the D630N mutant of HPAO is more active than the wild type, being one of a few cases where a single-point mutation increases the enzymatic rate. Second, the removal of a negative charge that interacts with a metal ligand has been shown to increase the redox potential of the copper center without changing the overall mechanism of oxygen activation. Last, the mutation has been proposed to alter the binding affinity of O_2 , possibly introducing an external commitment that reduces the ¹⁸O KIE values in relation to those of WT-HPAO. Copper centers are involved in a range of different biological processes, including O_2 transport, oxygenase, and oxidase reactions (21). Commonly, copper ions are coordinated by at least one histidine ligand. Hydrogen-bonding interactions of the copper-ligating histidine residues with the remainder of the protein can play an important part in controlling the reactivity of the metal center, as demonstrated herein. In the blue copper field, in particular, the major tuning of the redox potential of the active site copper has been shown to reside in the second-sphere ligands (39, 40).

ACKNOWLEDGMENT

We thank Dr. Junko Yano (University of California, Berkeley) for assistance with the EPR experiments and Bryan

Johnson and Professor Carrie Wilmot (University of Minnesota) for valuable discussions.

SUPPORTING INFORMATION AVAILABLE

A sequence alignment of the C-terminal portion of the copper amine oxidases, a depiction of the active site of HPAO, and UV–vis spectra of species that accumulate in the steady state for D630N. This information is available free of charge via the Internet at <http://pubs.acs.org>.

REFERENCES

- Mure, M., Mills, S. A., and Klinman, J. P. (2002) Catalytic mechanism of the topa quinone containing copper amine oxidases, *Biochemistry* 41, 9269–9278.
- Mure, M. (2004) Tyrosine-derived quinone cofactors, *Acc. Chem. Res.* 37, 131–139.
- Vandijken, J. P., and Bos, P. (1981) Utilization of Amines by Yeasts, *Arch. Microbiol.* 128, 320–324.
- Cona, A., Rea, G., Angelini, R., Federico, R., and Tavladoraki, P. (2006) Functions of amine oxidases in plant development and defence, *Trends Plant Sci.* 11, 80–88.
- O'sullivan, J., Unzeta, M., Healy, J., O'sullivan, M. I., Davey, G., and Tipton, K. F. (2004) Semicarbazide-sensitive amine oxidases: Enzymes with quite a lot to do, *Neurotoxicology* 25, 303–315.
- Salmi, M., and Jalkanen, S. (2001) VAP-1: an adhesin and an enzyme, *Trends Immunol.* 22, 211–216.
- Dubois, J. L., and Klinman, J. P. (2005) Mechanism of post-translational quinone formation in copper amine oxidases and its relationship to the catalytic turnover, *Arch. Biochem. Biophys.* 433, 255–265.
- Janes, S. M., Mu, D., Wemmer, D., Smith, A. J., Kaur, S., Maltby, D., Burlingame, A. L., and Klinman, J. P. (1990) A New Redox Cofactor in Eukaryotic Enzymes - 6-Hydroxydopa at the Active-Site of Bovine Serum Amine Oxidase, *Science* 248, 981–987.
- Brazeau, B. J., Johnson, B. J., and Wilmot, C. M. (2004) Copper-containing amine oxidases. Biogenesis and catalysis; a structural perspective, *Arch. Biochem. Biophys.* 428, 22–31.
- Dawkes, H. C., and Phillips, S. E. V. (2001) Copper amine oxidase: cunning cofactor and controversial copper, *Curr. Opin. Struct. Biol.* 11, 666–673.
- Airenne, T. T., Nymalm, Y., Kidron, H., Smith, D. J., Pihlavisto, M., Salmi, M., Jalkanen, S., Johnson, M. S., and Salminen, T. A. (2005) Crystal structure of the human vascular adhesion protein-1: Unique structural features with functional implications, *Protein Sci.* 14, 1964–1974.
- Jakobsson, E., Nilsson, J., Ogg, D., and Kleywegt, G. J. (2005) Structure of human semicarbazide-sensitive amine oxidase/vascular adhesion protein-1, *Acta Crystallogr., D* 61, 1550–1562.
- Agostinelli, E., Belli, F., Dalla Vedova, L., Longu, S., Mura, A., and Floris, G. (2005) Catalytic properties and the role of copper in bovine and lentil seedling copper/quinone-containing amine oxidases: Controversial opinions, *Eur. J. Inorg. Chem.* 1635–1641.
- Pietrangeli, P., Nocera, S., Mondovi, B., and Morpurgo, L. (2003) Is the catalytic mechanism of bacteria, plant, and mammal copper-TPQ amine oxidases identical?, *Biochim. Biophys. Acta—Proteins Proteomics* 1647, 152–156.
- Padiglia, A., Medda, R., Bellelli, A., Agostinelli, E., Morpurgo, L., Mondovi, B., Agro, A. F., and Floris, G. (2001) The reductive and oxidative half-reactions and the role of copper ions in plant and mammalian copper-amine oxidases, *Eur. J. Inorg. Chem.* 35–42.
- Dooley, D. M., Mcguirl, M. A., Brown, D. E., Turowski, P. N., McIntire, W. S., and Knowles, P. F. (1991) A Cu(I)-Semicarbazide State in Substrate-Reduced Amine Oxidases, *Nature* 349, 262–264.
- Shepard, E. M., and Dooley, D. M. (2006) Intramolecular electron transfer rate between active-site copper and TPQ in *Arthrobacter globiformis* amine oxidase, *J. Biol. Inorg. Chem.* 11, 1039–1048.
- Dooley, D. M., and Brown, D. E. (1996) Intramolecular electron transfer in the oxidation of amines by methylamine oxidase from *Arthrobacter P1*, *J. Biol. Inorg. Chem.* 1, 205–209.
- Turowski, P. N., Mcguirl, M. A., and Dooley, D. M. (1993) Intramolecular Electron-Transfer Rate between Active-Site Copper

- and Topa Quinone in Pea Seedling Amine Oxidase, *J. Biol. Chem.* 268, 17680–17682.
20. Lewis, E. A., and Tolman, W. B. (2004) Reactivity of dioxygen-copper systems, *Chem. Rev.* 104, 1047–1076.
 21. Mirica, L. M., Ottenwaelde, X., and Stack, T. D. P. (2004) Structure and spectroscopy of copper-dioxygen complexes, *Chem. Rev.* 104, 1013–1045.
 22. Goto, Y., and Klinman, J. P. (2002) Binding of dioxygen to non-metal sites in proteins: Exploration of the importance of binding site size versus hydrophobicity in the copper amine oxidase from *Hansenula polymorpha*, *Biochemistry* 41, 13637–13643.
 23. Su, Q. J., and Klinman, J. P. (1998) Probing the mechanism of proton coupled electron transfer to dioxygen: The oxidative half-reaction of bovine serum amine oxidase, *Biochemistry* 37, 12513–12525.
 24. Mills, S. A., Goto, Y., Su, Q. J., Plastino, J., and Klinman, J. P. (2002) Mechanistic comparison of the cobalt-substituted and wild-type copper amine oxidase from *Hansenula polymorpha*, *Biochemistry* 41, 10577–10584.
 25. Mills, S. A., and Klinman, J. P. (2000) Evidence against reduction of Cu²⁺ to Cu⁺ during dioxygen activation in a copper amine oxidase from yeast, *J. Am. Chem. Soc.* 122, 9897–9904.
 26. De Matteis, G., Agostinelli, E., Mondovi, B., and Morpurgo, L. (1999) The metal function in the reactions of bovine serum amine oxidase with substrates and hydrazine inhibitors, *J. Biol. Inorg. Chem.* 4, 348–353.
 27. Kishishita, S., Okajima, T., Kim, M., Yamaguchi, H., Hirota, S., Suzuki, S., Kuroda, S., Tanizawa, K., and Mure, M. (2003) Role of copper ion in bacterial copper amine oxidase: Spectroscopic and crystallographic studies of metal-substituted enzymes, *J. Am. Chem. Soc.* 125, 1041–1055.
 28. Mura, A., Padiglia, A., Medda, R., Pintus, F., Agro, A. F., and Floris, G. (2006) Properties of copper-free pig kidney amine oxidase: Role of topa quinone, *FEBS Lett.* 580, 4317–4324.
 29. Padiglia, A., Medda, R., Pedersen, J. Z., Agro, A. F., Lorrain, A., Murgia, B., and Floris, G. (1999) Effect of metal substitution in copper amine oxidase from lentil seedlings, *J. Biol. Inorg. Chem.* 4, 608–613.
 30. Prabhakar, R., and Siegbahn, P. E. M. (2004) A theoretical study of the mechanism for the biogenesis of cofactor topaquinone in copper amine oxidases, *J. Am. Chem. Soc.* 126, 3996–4006.
 31. Prabhakar, R., Siegbahn, P. E. M., and Minaev, B. F. (2003) A theoretical study of the dioxygen activation by glucose oxidase and copper amine oxidase, *Biochim. Biophys. Acta—Proteins Proteomics* 1647, 173–178.
 32. Juda, G. A., Shepard, E. M., Elmore, B. O., and Dooley, D. M. (2006) A comparative study of the binding and inhibition of four copper-containing amine oxidases by azide: Implications for the role of copper during the oxidative half-reaction, *Biochemistry* 45, 8788–8800.
 33. Medda, R., Padiglia, A., Bellelli, A., Sarti, P., Santanche, S., Agro, A. F., and Floris, G. (1998) Intermediates in the catalytic cycle of lentil (*Lens esculenta*) seedling copper-containing amine oxidase, *Biochem. J.* 332, 431–437.
 34. Cai, D. Y., and Klinman, J. P. (1994) Copper Amine Oxidase—Heterologous Expression, Purification, and Characterization of an Active Enzyme in *Saccharomyces-Cerevisiae*, *Biochemistry* 33, 7647–7653.
 35. Dubois, J. L., and Klinman, J. P. (2004) Methods for characterizing TPQ-containing proteins, *Methods Enzymol.* 378, 17–31.
 36. Tian, G. C., and Klinman, J. P. (1993) Discrimination between O-16 and O-18 in Oxygen-Binding to the Reversible Oxygen Carriers Hemoglobin, Myoglobin, Hemerythrin, and Hemocyanin—a New Probe for Oxygen-Binding and Reductive Activation by Proteins, *J. Am. Chem. Soc.* 115, 8891–8897.
 37. Mure, M., and Klinman, J. P. (1993) Synthesis and Spectroscopic Characterization of Model Compounds for the Active-Site Cofactor in Copper Amine Oxidases, *J. Am. Chem. Soc.* 115, 7117–7127.
 38. Hess, C. R., Juda, G. A., Dooley, D. M., Amii, R. N., Hill, M. G., Winkler, J. R., and Gray, H. B. (2003) Gold electrodes wired for coupling with the deeply buried active site of *Arthrobacter globiformis* amine oxidase, *J. Am. Chem. Soc.* 125, 7156–7157.
 39. Machczynski, M. C., Gray, H. B., and Richards, J. H. (2002) An outer-sphere hydrogen-bond network constrains copper coordination in blue proteins, *J. Inorg. Biochem.* 88, 375–380.
 40. Crane, B. R., Di Bilio, A. J., Winkler, J. R., and Gray, H. B. (2001) Electron tunneling in single crystals of *Pseudomonas aeruginosa* azurins, *J. Am. Chem. Soc.* 123, 11623–11631.
 41. Dooley, D. M., Scott, R. A., Knowles, P. F., Colangelo, C. M., Mcguirl, M. A., and Brown, D. E. (1998) Structures of the Cu(I) and Cu(II) forms of amine oxidases from x-ray absorption spectroscopy, *J. Am. Chem. Soc.* 120, 2599–2605.
 42. Li, R. B., Klinman, J. P., and Mathews, F. S. (1998) Copper amine oxidase from *Hansenula polymorpha*: the crystal structure determined at 2.4 angstrom resolution reveals the active conformation, *Structure* 6, 293–307.
 43. Bellelli, A., Agro, A. F., Floris, G., and Brunori, M. (1991) On the Mechanism and Rate of Substrate Oxidation by Amine Oxidase from Lentil Seedlings, *J. Biol. Chem.* 266, 20654–20657.
 44. Takahashi, K., and Klinman, J. P. (2006) Relationship of stopped flow to steady state parameters in the dimeric copper amine oxidase from *Hansenula polymorpha* and the role of zinc in inhibiting activity at alternate copper-containing subunits, *Biochemistry* 45, 4683–4694.
 45. Steinebach, V., Devries, S., and Duine, J. A. (1996) Intermediates in the catalytic cycle of copper-quinoprotein amine oxidase from *Escherichia coli*, *J. Biol. Chem.* 271, 5580–5588.
 46. Roth, J. P. (2007) Advances in Studying Bioinorganic Reaction Mechanisms: Isotopic Probes of Activated Oxygen Intermediates in Metalloenzymes, *Curr. Opin. Chem. Biol.* 11, 142–150.

BI700943R